RESEARCH PAPER

Effect of Heat-Treatment Temperatures on Magnetite Oxidation in $20SiO_2.50FeO.30CaO$ Glass Ceramic Prepared by the Sol-Gel Method

Parisa Rastgoo Oskoui, Mahammad Rezvani*, Abbas Kianvash

* *m_rezvani@tabrizu.ac.ir*

[1] Department of Materials Engineering, University of Tabriz, Tabriz, Iran

Received: April 2023 **Revised: May 2023** **Accepted: June 2023**
DOI: 10.22068/ijmse.3238

Abstract: *The effect of different heat-treatment temperatures on the magnetic, crystallization, and structural properties of $20SiO_2.50FeO.30CaO$ (mol%) glass ceramics was studied. The initial glass was synthesized by the sol-gel method at 25°C with a precursor to solvent ratio of 1/5. After aging the resulting gel for 24 h at room temperature, it was dried in an electric dryer at 110°C. By heat treatment at different temperatures, different phases such as magnetite, maghemite, and hematite were crystallized in the glass. The maximum stability temperature of magnetite and maghemite were 360°C and 440°C respectively. By increasing the heat treatment temperature to higher than 440°C, the oxidation of maghemite to hematite was occurred. The highest magnetization amount (1.9 emu/g) belonged to sample heat treated at 680°C. By increasing the heat treatment temperature to 840°C, the magnetization decreased to 0.8 emu/g, due to the oxidation of maghemite. By increasing the heat treatment temperature from 440°C to 680°C, crystalline size of maghemite was increased from 40 to 200 nm. By further increment of temperature to 840°C, the size of maghemite crystals decreased to 17 nm, due to the oxidation of maghemite to hematite.*

Keywords: *Bioactive Glass-Ceramic, Magnetic properties, Sol-Gel, Hyperthermia, Maghemite.*

1. INTRODUCTION

Although the prevalence of malignant bone tumors is low, the mortality rate of this disease is high [1]. This disease is mainly treated with traditional method such as surgery, chemotherapy, and radiotherapy. Surgery is an invasive procedure with high complications. Risk of infection in the surgical procedure as a result of the removal of tumor-containing tissue or amputation and reconstruction of the removed tissue with implants are pervasive in patients who are already immunocompromised [2].

To overcome these problems, new methods such as immunotherapy (gene therapy, etc.) have been developed [3]. One of the new solutions is the magnetic hyperthermia method. In this method, heat is used to destroy cancerous tumors. In the magnetic fluid hyperthermia method, the temperature of the cancerous tumor increases up to 43°C. With the temperature increasing up to this range, cancer cells are destroyed, while healthy cells are not harmed [4].

The difference between the behavior of tumors and normal tissue against the application of body heat depends on their vascular network [5]. The temperature applied in the range of 41-43°C is lethal for tumor cells, while it does not harm normal cells. The difference in the therapeutic effect of hyperthermia between normal and malignant tissue, basically depends on the structure of the vascular network of these two. Also, the tissue of tumors and their response to hyperthermia has a significant effect [6].

Recently, magnetic nanoparticles such as Fe_3O_4 have been used as heat generators for magnetic hyperthermia. These nanoparticles have excellent chemical stability and magnetic properties. But metal oxide nanoparticles may have dangerous interactions with the biological systems of the human body and eventually lead to toxicity that would not be safe for medical applications [7].

On the other hand, these nanoparticles have high saturation magnetization and very little coercivity, and this causes nanoparticles to have high rate of loss under the magnetic field. An excessive increase in temperature (temperatures above 45°C) under an alternating magnetic field also leads to the destruction of healthy cells [8]. Because of these issues in magnetic hyperthermia, more research continues in magnetic glass ceramics [9, 10].

Magnetic bioactive glass ceramics are complex and multiphase bioactive materials typically formed by combining bioglass with the magnetic phase [11]. The bioactivity of biocompatible magnetic glass ceramics is attributed to the formation of bone minerals such as apatite

[DOI: 10.22068/ijmse.3238]

in the simulated body solution [12]. Different researchers have synthesized different ferromagnetic glass ceramics in different systems, such as, SiO_2- Na_2O- CaO-P_2O_5- FeO- Fe_2O_3 [9], SiO_2- CaO- Fe_2O_3 [13], SiO_2- Fe_2O_3- Li_2O- CaO- MnO_2- P_2O_5 [14], SiO_2- CaO- Fe_2O_3- B_2O_3- P_2O_5 [15], SiO_2- CaO- P_2O_5- Fe_2O_3- ZnO- Na_2O [16, 17], SiO_2- CaO- P_2O_5- MgO- CaF_2- MnO_2- Fe_2O_3 [18-20], SiO_2- CaO- Fe_2O_3- ZnO [21] with controlled crystallization.

The most important challenge in the synthesis of bioactive magnetic glass ceramics is the synthesis of amorphous glass and the crystallization of magnetic phases to achieve high magnetic saturation (M_s), at the same time a low coercivity (H_c) and remanence (M_r). Different researchers have reported different values for magnetic saturation magnetization (M_s), coercivity (H_c), and remanence (M_r) of glass-ceramic samples due to heat treatment at different temperatures [22-25].

The heating of magnetic glass ceramic under an alternating magnetic field is mainly due to hysteresis and the Brownian relaxation losses. If the effect of Brownian losses is considered negligible, particles undergoing significant alternating magnetic fields will have high hysteresis losses [26]. On the other hand, the hysteresis loss is directly related to the area of the magnetic hysteresis loop, and the greater the area of the hysteresis loop causes the magnetic loss is greater [27, 28].

Therefore, the main goal of this research was to study the effect of different heat treatment temperatures on the crystallization of different magnetic phases and to investigate the magnetic properties of $20SiO_2.50FeO.30CaO$ samples.

2. EXPERIMENTAL PROCEDURES

2.1. Synthesis of Sol-Gel Bioactive Glass

The glass was synthesized by the self-catalyzing sol method [29]. Briefly, 4.2 ml tetraethyl orthosilicate (TEOS, $Si(OC_2H_5)_4$; 99%, Merck) was stirred in 12 ml ethanol C_2H_5OH; 98%, Sigma Aldrich) for 20 minutes. Then 6.5 gr calcium nitrate tetrahydrate ($Ca(NO_3)_2.4H_2O$; 99.5%, Merck) dissolved in 25 ml distilled water was added to the reaction chamber, and after stirring for 30 minutes, 8.6 iron nitrate ($FeNO_3$; 99%, Sigma Aldrich) dissolved in 13 ml ethanol was added to the sol. Stirring continued for 1 h. The obtained sol was stored for 24 h in a closed container at room temperature for gelation aging process. Then, the resulted gel was dried in a dryer at a temperature of 110°C for 24 h. The obtained powder was heat treated at 280, 360, 440, 520, 600, 680, 760, 840°C, separately, for 2 h in an air atmosphere. Then phase, structural and magnetic analysis were performed on the samples.

2.2. Sample Analysis

The crystallinity of the samples were investigated using an Empyrean Series 2 diffractometer manufactured by PANalytical, (Malvern, UK), with Cu K_α radiation. Phase detection was performed using X'Pert HighScore v.4. software (PANalytical, Malvern, UK). The size of the crystallized crystals in the glass-ceramic was calculated using the Debye-Scherrer relation:

$$d = \frac{K\lambda}{\beta\cos\theta} \quad (1)$$

Where λ is the wavelength of the X-ray in nanometers (nm), β is the full width at half maximum, and the constant K related to the crystal shape and its value is usually considered to be 0.9. The value of β in the 2θ axis of the diffraction profile should be in radians [30].

FTIR spectroscopy of heat-treated samples at different temperatures was performed using a JASCO FT/IR-300E spectrophotometer (JASCO, Japan). The samples prepared using the KBr technique were examined at room temperature at 400-4000 cm^{-1}. EPR spectroscopy of glass-ceramic powder samples were performed at room temperature using Adani CMS 8400 (Adani, Minsk, Belarus). The glass-ceramic powder was poured into a quartz tube with a diameter of 4.0 mm. Sample volumes varied from 2.0 to 5.0 mm, and spectra were recorded with an ultra-high-Q rectangular resonator (Bruker Optik GmbH, Ettlingen, Germany). To calibrate the absolute values of g factors, chromium chloride $CrCl_3$ (S= 2.3) with g= 1.986 was used. The samples morphology were investigated by Scanning Electron Microscopy equipped with Energy Dispersive Spectroscopy (SEM-EDS, SEM-FEI, Quanta Inspect 200, EDS-EDAX PV 9900).

3. RESULTS AND DISCUSSION

Fig. 1 shows the XRD patterns of dried gel and the heat-treated samples at 280 and 360°C. XRD pattern of the dried gel shows its amorphous

[DOI: 10.22068/ijmse.3238]

nature. By performing heat treatment at 280°C, only the magnetite phase has crystallized. With increasing the heat treatment temperature, the intensity of the peaks related to the magnetite phase has increased. It seems that no other phase except magnetite was crystalized in the sample. According to the observed absorption intensity caused by the background, it seems that the amorphous background is remained in the glass-ceramics.

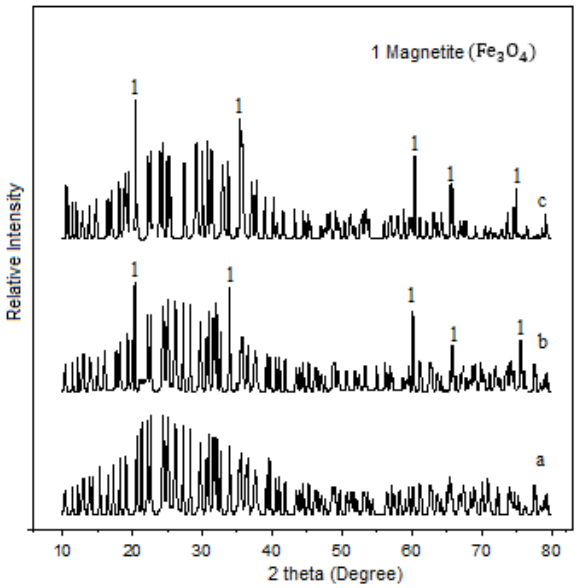

Fig. 1. XRD patterns of $20SiO_2.50FeO.30CaO$ glasses a) dried gel, b) heat-treated at 280 and c) 360°C.

The FTIR patterns of heat-treated samples at 280 and 360°C is shown in Fig. 2. The absorption band related to the symmetric stretching vibrations of Si-O-Si can be seen in the range of 1015 cm^{-1} wavenumber, and the position of this peak has not changed significantly with increasing temperature. Asymmetric stretching vibrations of $[Si-O]^-$ are seen in of 916 cm^{-1}.With increasing of the heat-treatment temperature, the position of this peak has shifted to lower wavenumbers. Iron ions in percentages higher than 30% by weight act as a network former in the glass network [31, 32]. As the heat-treatment temperature and the crystallization rate of the magnetite phase increases, the residual glass becomes poor in iron, and rich in modifier ions. These events lead to breaking up of the glass network. As a result, the absorption bands related to the asymmetric stretching vibrations of Si-O-NBO have shifted to smaller wavenumbers. The absorption band in 560 cm^{-1} is related to crystalline magnetite phase [33, 34]. It is also seen that the intensity of this peak has increased with heat treatment temperature, which means an increase in the number of bonds formed and/or an increase in the amount of magnetite.

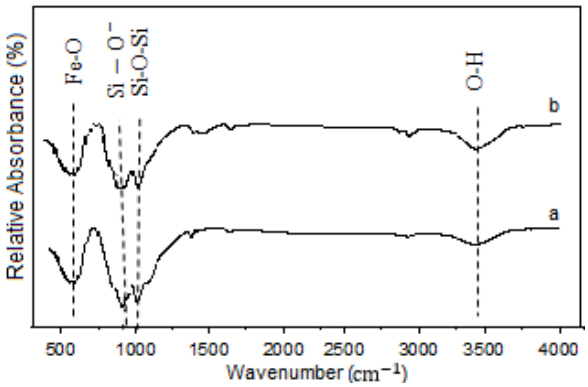

Fig. 2. FTIR patterns of $20SiO_2.50FeO.30CaO$ glass heat-treated at a) 280 and b) 360°C.

The results of the XRD patterns of heat-treated samples at 440°C and 520°C are depicted in Fig. 3. It can be seen from this figure that by heat treating at 440°C, magnetite peaks are completely removed, and maghemite peaks have appeared. Crystallized maghemite has a cubic crystal structure with symmetry group $p4_332$. When the heat-treatment temperature has increased to 520°C, hematite crystals have started to form in the glass matrix.

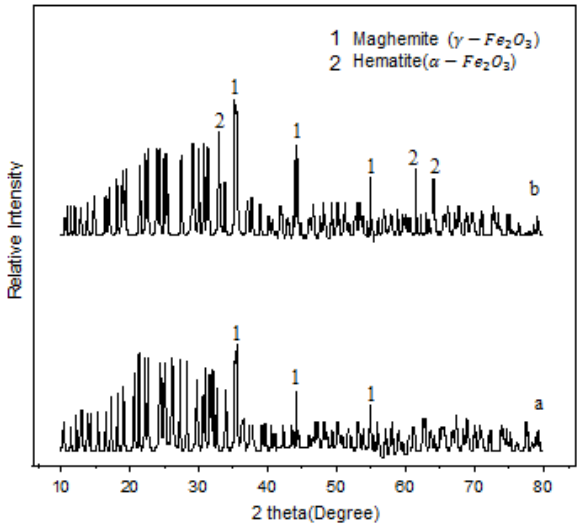

Fig. 3. XRD patterns of $20SiO_2.50FeO.30CaO$ glass heat treated at a) 440°C and b) 520°C.

A lot of studies have been done on the transformation of magnetite to maghemite or hematite (relationship), which can be done

[DOI: 10.22068/ijmse.3238]

partially or completely depending on the oxidation state:

$4Fe_3O_4 + O_2 \rightarrow 6\gamma Fe_2O_3 \rightarrow 6\alpha Fe_2O_3$

With increasing the temperature, magnetite oxidized to maghemite, while the amount of maghemite increases and the percentage of magnetite decreases [35].

Magnetite has a cubic inverted spinel crystal structure with the symmetry group of $Fd\bar{3}m$. Furthermore oxygen ions, alongside with divalent and trivalent iron ions exist in its structure. While in maghemite, only oxygen ions, trivalent iron, along and available exist in the structure. Depending on the position of vacancies in the crystal structure, different crystal structures are formed. If the vacancies are irregularly placed in the crystal structure, maghemite will be formed with a cubic crystal system and symmetry group of $p4_332$. As oxidation process continues, the positions of the vacancies in the crystal structure become balanced. The vacancies in the crystal structure expand in a completely regular manner. As a result, maghemite will be crystallized with a tetragonal crystal structure and spatial symmetry group of $P4_12_12$. It is possible to identify and monitor the position of vacancies in the maghemite crystal structure using X-ray diffraction patterns and FTIR spectra. As the oxidation process finalizes, maghemite completely transforms into hematite, and hematite crystallizes with a trigonal crystal structure and rhombohedral space group of $R\bar{3}c$ [36-38].

FTIR spectrum of heat-treated samples at 440°C and 520°C are shown in Fig. 4. In the heat-treated sample at 440°C, maghemite absorption bands with a cubic crystal system and symmetric group of $p4_332$ are seen at 465 and 571 cm^{-1} wavenumbers [39-41], which is in line with the investigations carried out by X-ray diffraction spectra. In the heat-treated sample at 520°C, absorption bands of maghemite with tetragonal crystal structure and space symmetry group $P4_12_12$ were seen. Absorption bands of maghemite with tetragonal crystal structure and spacial symmetric group of $P4_12_12$ are seen at 472, 440 cm^{-1}, and 560 cm^{-1} positions [42, 43]. In the spectrum of the heat-treated sample at 520°C, hematite absorption bands are seen at 520 cm^{-1} and 660 cm^{-1} wavenumbers.

With the increase the temperature, a difference in the crystal structure of maghemite can be seen. This difference denotes the maximum stability of ferromagnetic maghemite crystals in the glass structure at 440°C. With a further increasing of the heat-treatment temperature, the crystal structure changes towards formation of hematite. Both maghemite and magnetite have similar crystal structures, and their structural differences are little. According to the investigations, these transformations occur with the penetration of ions in the solid state in two modes: the first mode occurs by the penetration of oxygen ions towards the magnetite crystals, and the second mode occurs by the penetration of iron atoms to the crystal outside, which leads to the formation of $Fe_{3-x}O_4$ solid solution or a core-shell structure made of magnetite- maghemite as a result of the oxidation of iron ions on the surface of particles. The migration of iron ions to new surfaces is done quickly, but this speed is not high enough to fill the cation vacancies [44]. Considering the fact that the conversion of magnetite to maghemite is dependent on the penetration of iron ions, the speed of this penetration is the dominating factor of magnetite decomposition [45].

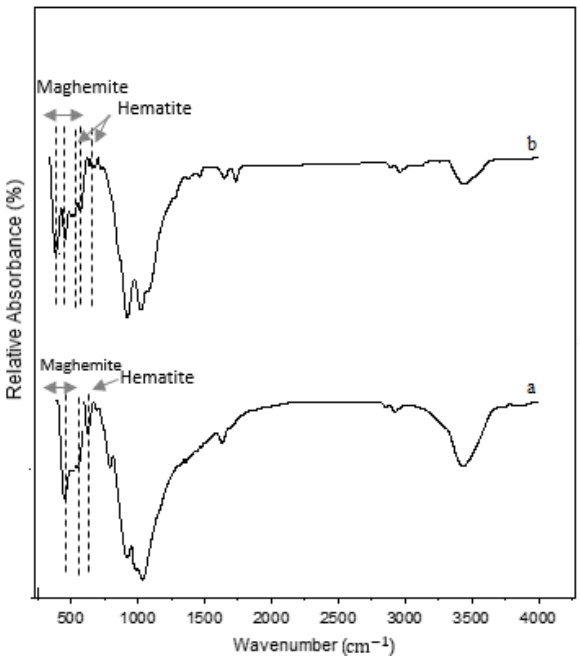

Fig. 4. FTIR patterns of $20SiO_2.50FeO.30CaO$ glass heat-treated at temperatures a) 440°C and b) 520°C.

The XRD patterns of samples heat-treated at 600, 680, and 760°C are shown in Fig. 5. According to the patterns, the intensity of hematite and

[DOI: 10.22068/ijmse.3238]

maghemite peaks increase with the increment of heat -treatment temperature. The increase in the intensity of hematite peaks at 760°C indicates that the major part of maghemite has been transformed into hematite at higher temperatures.

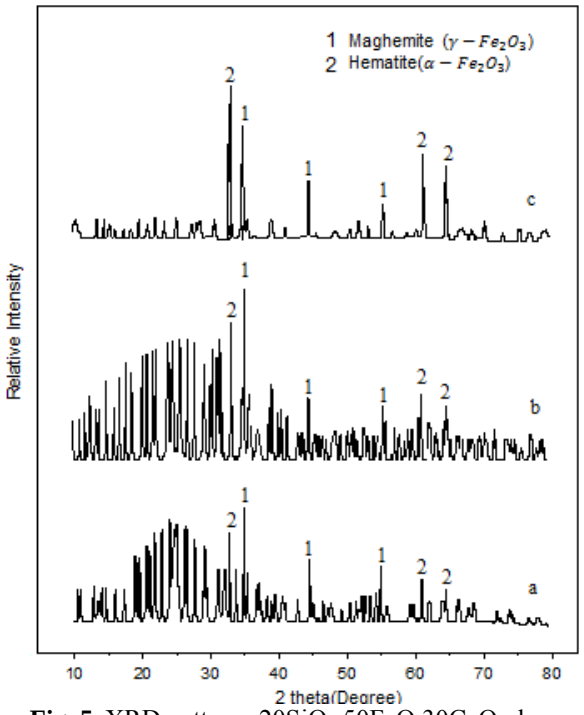

Fig. 5. XRD patterns $20SiO_2.50FeO.30CaO$ glass heat-treated at a) 600°C, b) 680°C, and c) 760°C.

The XRD patterns of samples heat-treated at 840°C and 920°C can be seen in Fig. 6. By increasing the heat treatment temperature up to 840°C, wollastonite, magnetite, hematite, and sodium calcium silicate phases are crystalized. At 920°C, only wollastonite and fayalite phases are crystalized. Using Scherer's relation, the size of maghemite and hematite crystals at different heat-treatment temperatures are calculated and shown in Fig. 7. By increasing the heat treatment temperature from 440°C to 680°C, the size of maghemite crystals increase from 40 to 200 nm due to the increase in penetration and atomic movements. By increasing the temperature to 840°C, the size of maghemite crystals has decreased to 17 nm, due to the oxidation of maghemite to hematite. The size of the hematite crystals increases with the increment of heat treatment temperature because of higher penetration the glass network.

The magnetization diagram of $20SiO_2.50FeO30CaO$ glass-ceramic samples, subjected to heat-treatment at different temperatures, are shown in Fig. 8. The highest value of magnetic saturation corresponds to the heat-treated sample at 680°C. With the increase in heat-treatment temperature (from 440°C to 680°C) due to the increase in penetration of atoms, the amount of maghemite crystallization has increased. As a result, it has led to an increase in the amount of magnetization. At temperatures higher than 680°C, magnetic saturation decreases, due to the transformation of maghemite into hematite.

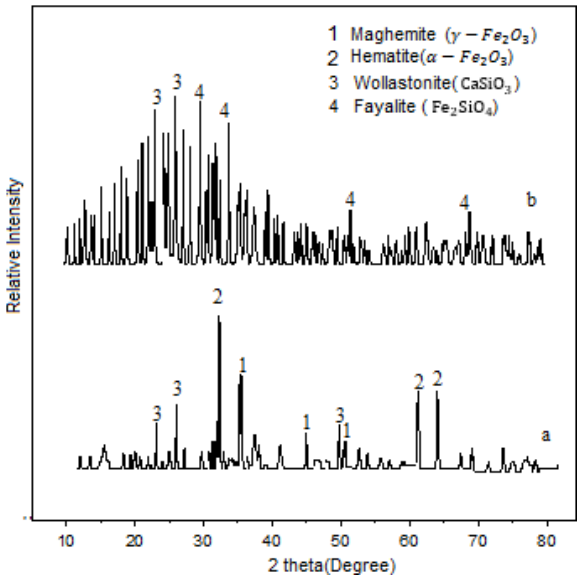

Fig. 6. XRD patterns of $20SiO_2.50FeO.30CaO$ glass heat-treated at a) 840°C and b) 920°C.

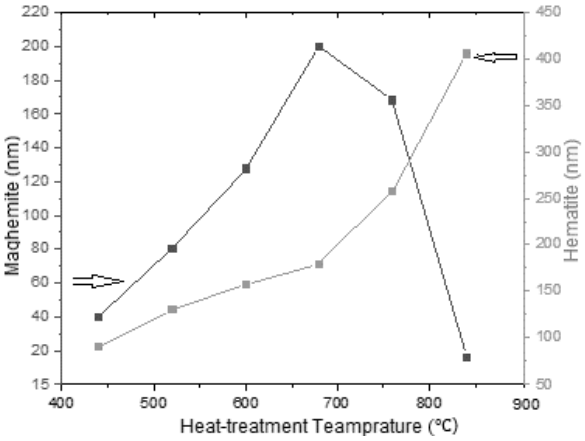

Fig. 7. The relationship between maghemite and hematite crystal size and heat treatment temperature.

Remanence magnetism is a natural quantity that reflects the fact that glass ceramics can be spontaneously magnetized even in the absence of an external magnetic field [46].

[DOI: 10.22068/ijmse.3238]

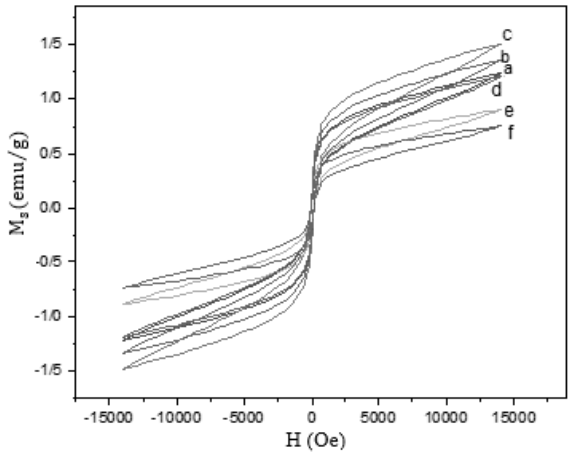

Fig. 8. Magnetization diagram (VSM) of $20SiO_2$-50FeO-30CaO glass-ceramic samples heat treated at a) 520°C, b) 600°C, c) 680°C, d) 440°C, e) 760°C and f) 840°C.

And this value is much lower than saturation magnetic values due to the structural characteristics of glass-ceramics. Remanence magnetism, as well as coercivity, strongly depends on the microstructure of the glass ceramic and the size of the crystalline phases [47]. It can also be seen that none of the samples have reached the saturation state, meaning that all the iron cations have not crystallized in the glass matrix and still paramagnetic ions are available in the glass. The changes in magnetic parameters of heat-treated glass-ceramics at different temperatures are shown in Fig. 9.

Room temperature EPR spectra of $20SiO_2.50FeO.30CaO$ glass heat-treated at various temperatures are shown in Fig. 10. It can be seen that heat treatment strongly affects the absorption spectra of samples. Fe^{3+} ions shows a resonance absorption at g~ 2.1 and 4.3 [48]. In general, the presence of Fe^{3+} ions in glass-ceramics is identified by the appearance of resonance absorptions at g~ 4.3 and 2.1. In these resonance absorptions, their line width and relative intensity depend on the concentration of iron oxide in the sample [49]. Isolated Fe^{3+} ions in distorted rhombic octahedral or tetrahedral oxygen environments lead to resonant absorption at g~ 4.3. While the ions that are clustered in the structure and interact by a superexchange pair lead to resonance absorption in g~ 2.1. In general, the interaction between Fe^{3+} and Fe^{2+} ions tends to expand the absorption line width. Also, superexchange mechanisms between ions tend to narrow the absorption line. The relative strengths of these two mechanisms will determine the final line width. It can be seen that the width of the absorption line in g~ 2.1 has increased with the increase in heat treatment temperature, which indicates the increase in the concentration of Fe^{2+} ions in glass-ceramics. Increasing the concentration of Fe^{2+} ions in the glass-ceramic composition has led to an increase in the crystallization of the hematite phase and, ultimately, to a decrease in the magnetic properties of the samples.

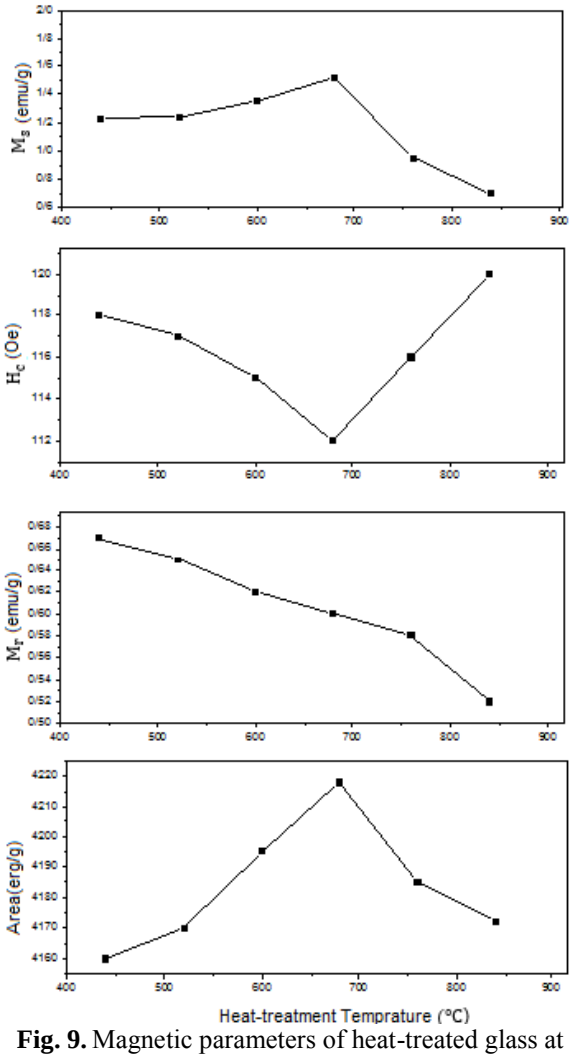

Fig. 9. Magnetic parameters of heat-treated glass at various temperatures.

SEM images of heat-treated samples at different temperatures are shown in Fig. 11. In the heat-treated sample at 440°C, maghemite crystallized with a rod-like morphology [50, 51], and with the increase of the heat-treatment temperature to

[DOI: 10.22068/ijmse.3238]

520°C, the size of maghemite crystals increased. Hematite polyhedral crystals can be seen [52, 53]. By heat-treatment at temperatures higher than 600°C, maghemite with rod-like morphology is crystallized in the matrix, and as a result of maghemite oxidation, hematite with a polyhedral morphology is formed.

In the image related to the heat-treated sample at 760°C, it is clearly seen that the amount of maghemite and hematite crystals have decreased and increased respectively. In the heat-treated sample at 840°C, hematite crystals clearly have grown and small amounts of maghemite crystals can be seen.

4. CONCLUSIONS

20SiO.50FeO.30CaO glass ceramic was synthesized by self-catalyzed sol method. Heat treatment of powders was done at different temperatures. By performing heat treatment at 280 and 360°C, only the magnetite phase crystallized in the samples. Due to the low temperature of the heat treatment and the low degree of crystallization of the glass ceramics, the magnetic properties of the samples were very weak and were negligible.

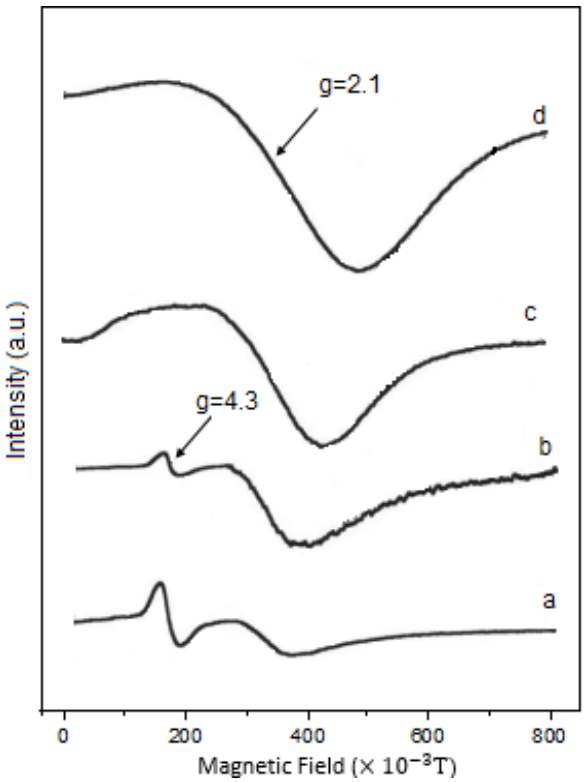

Fig. 10. Room temperature EPR spectra of $20SiO_2$-50FeO-30CaO glass ceramic heat-treated at various temperatures.(a) 440°C,(b) 520°C,(c) 600°C, d) 680°C.

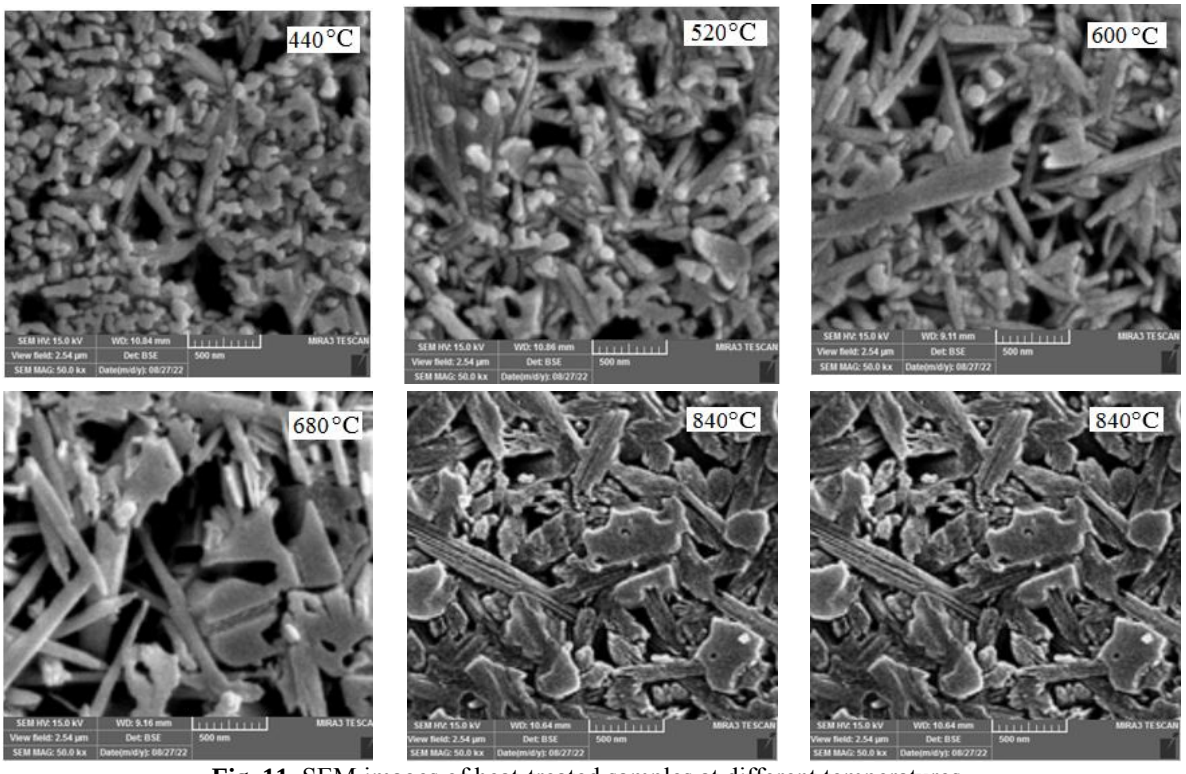

Fig. 11. SEM images of heat-treated samples at different temperatures.

[DOI: 10.22068/ijmse.3238]

By increasing the heat treatment temperature to 440°C, magnetite was oxidized to maghemite. The saturation magnetism of maghemite (80 emu/g) is lower than magnetite (90 emu/g). By increasing the heat treatment temperature to 520°C, the size of maghemite crystals increased. At this temperature also some part of the maghemite crystals were oxidized to hematite. Hematite is an antiferromagnetic phase, and the oxidation of maghemite to hematite led to a decrease in the magnetic properties of the samples.

The structural analysis showed that iron ions were present in the glass network as a network former. The highest stability temperature of the maghemite phase was 440°C and the highest saturation magnetization of the heat-treated sample was obtained at 680°C. The highest hysteresis loss was related to the sample heat treated at 680°C. Microstructural studies showed that in the samples heat treated at lower temperatures (≤680°C), maghemite was crystallized with a rod structure, and with increasing heat treatment temperature, maghemite turned into hematite.

ACKNOWLEDGEMENTS

The authors would like to acknowledge the support of Tabriz university for this research.

REFERENCES

[1] K.M. Zekry, N. Yamamoto, K. Hayashi, A. Takeuchi, A.Z.A. Alkhooly, A.S. Abd-Elfattah, A.N.S. Elsaid, A.R. Ahmed, H. Tsuchiya, "Reconstruction of intercalary bone defect after resection of malignant bone tumor", J. Orthop. Surg., 2019, 27, 2309499019832970.

[2] H. Xiang, Q. Yang, Y. Gao, D. Zhu, S. Pan, T. Xu, Y. Chen, "Cocrystal strategy toward multifunctional 3D-printing scaffolds enables NIR-activated photonic osteosarcoma hyperthermia and enhanced bone defect regeneration", Adv. Funct. Mater., 2020, 30, 1909938.

[3] I.W. Folkert, S. Devalaraja, G.P. Linette, K. Weber, M. Haldar, "Primary bone tumors: challenges and opportunities for CAR-T therapies", J. Bone Miner. Res., 2019, 34, 1780-1788.

[4] M. Chang, Z. Hou, M. Wang, C. Li, J. Lin, "Recent advances in hyperthermia therapy-based synergistic immunotherapy", Adv. Mater., 2021, 33, 2004788.

[5] J. Beik, Z. Abed, F.S. Ghoreishi, S. Hosseini-Nami, S. Mehrzadi, A. Shakeri-Zadeh, S.K. Kamrava, "Nanotechnology in hyperthermia cancer therapy: From fundamental principles to advanced applications", Int. J. Radiat. Oncol. Biol. Phys., 2016, 235, 205-221.

[6] M. Nabil, P. Zunino, "A computational study of cancer hyperthermia based on vascular magnetic nanoconstructs", R Royal Soc. Open Sci., 2016, 3, 160287.

[7] N. Malhotra, J.-S. Lee, R.A.D. Liman, J.M.S. Ruallo, O.B. Villaflores, T.-R. Ger, C.-D. Hsiao, "Potential toxicity of iron oxide magnetic nanoparticles: a review", Molecules, 2020, 25, 3159.

[8] V.V. Mody, A. Singh, B. Wesley, "Basics of magnetic nanoparticles for their application in the field of magnetic fluid hyperthermia", Eur. J. Nanomed, 2013, 5, 11-21.

[9] O. Bretcanu, E. Verné, M. Cöisson, P. Tiberto, P. Allia, "Magnetic properties of the ferrimagnetic glass-ceramics for hyperthermia", J. Appl. Biomater. Funct. Mater., 2006, 305, 529-533.

[10] S.A. Shah, M. Hashmi, S. Alam, A. Shamim, "Magnetic and bioactivity evaluation of ferrimagnetic $ZnFe_2O_4$ containing glass ceramics for the hyperthermia treatment of cancer", J. Magn. Magn. Mater., 2010, 322, 375-381.

[11] D. Arcos, R. Del Real, M. Vallet-Regı, "A novel bioactive and magnetic biphasic material", Biomaterials, 2002, 23, 2151-2158.

[12] G. Li, K. Zhang, Z. Pei, N. Zhang, Y. Yu, S. Zhao, G. Liang, J. Zhou, Y. Xing, "A novel method to enhance magnetic property of bioactive glass-ceramics for hyperthermia", Ceram. Int., 2019, 45, 4945-4956.

[13] R.K. Singh, G. Kothiyal, A. Srinivasan, "Magnetic and structural properties of $CaO–SiO_2–P_2O_5–Na_2O–Fe_2O_3$ glass ceramics", J. Magn. Magn. Mater., 2008, 320, 1352-1356.

[14] C.-S. Hsi, H.-Z. Cheng, H.-J. Hsu, Y.-S.

[DOI: 10.22068/ijmse.3238]

Chen, M.-C. Wang, "Crystallization kinetics and magnetic properties of iron oxide contained $25Li_2O–8MnO_2–20CaO–2P_2O_5–45SiO_2$ glasses", J. Eur. Ceram., 2007, 27, 3171-3176.

[15] G. Kothiyal, K. Sharma, A. Dixit, A. Srinivasan, "Structural and Magnetic Studies on Nano-crystalline Biocompatible Glass/Glass-ceramic", AIP Conf. Proc., 2010, 55-59.

[16] S.A. Shah, M. Hashmi, S. Alam, "Effect of aligning magnetic field on the magnetic and calorimetric properties of ferrimagnetic bioactive glass ceramics for the hyperthermia treatment of cancer", Mater. Sci. Eng. C., 2011, 31, 1010-1016.

[17] S.A. Abdel-Hameed, A.M. El Kady, "Effect of different additions on the crystallization behavior and magnetic properties of magnetic glass–ceramic in the system $Fe_2O_3–ZnO–CaO–SiO_2$", J. Adv. Res., 2012, 3, 167-175.

[18] R.K. Singh, A. Srinivasan, G. Kothiyal, "Evaluation of $CaO–SiO_2–P_2O_5–Na_2O–Fe_2O_3$ bioglass-ceramics for hyperthermia application", J Mater Sci Mater Med, 2009, 20, 147-151.

[19] R.K. Singh, A. Srinivasan, "Bioactivity of ferrimagnetic $MgO–CaO–SiO_2–P_2O_5–Fe_2O_3$ glass-ceramics", Ceram. Int., 2010, 36, 283-290.

[20] S.A. Abdel-Hameed, M.A. Marzouk, M.M. Farag, "Effect of P_2O_5 and MnO_2 on crystallization of magnetic glass ceramics", J. Adv. Res., 2014, 5, 543-550.

[21] S.C. von Clausbruch, M. Schweiger, W. Höland, V. Rheinberger, "The effect of P_2O_5 on the crystallization and microstructure of glass-ceramics in the $SiO_2–Li_2O–K_2O–ZnO–P_2O_5$ system", J. Non Cryst Solids, 2000, 263, 388-394.

[22] F. Baino, E. Fiume, M. Miola, F. Leone, B. Onida, F. Laviano, R. Gerbaldo, E. Verné, "Fe-doped sol-gel glasses and glass-ceramics for magnetic hyperthermia", Materials, 2018, 11, 173.

[23] K. Mahmoudi, A. Bouras, D. Bozec, R. Ivkov, C. Hadjipanayis, "Magnetic hyperthermia therapy for the treatment of glioblastoma: a review of the therapy's history, efficacy and application in humans", Int. J. Hyperthermia, 2018, 34, 1316-1328.

[24] S. Gavazzi, A.L. van Lier, C. Zachiu, E. Jansen, J.J.W. Lagendijk, L.J.A. Stalpers, H. Crezee, H.P. Kok, "Advanced patient-specific hyperthermia treatment planning", Int. J. Hyperthermia, 2020, 37, 992-1007.

[25] A. Yazdanpanah, F. Moztarzadeh, S. Arabyazdi, "A heat-generating lithium-ferrite doped bioactive glass for cancer hyperthermia", Phys. Rev. B Condens. Matter, 2020, 593, 412298.

[26] G. Vallejo-Fernandez, O. Whear, A. Roca, S. Hussain, J. Timmis, V. Patel, K. O'grady, "Mechanisms of hyperthermia in magnetic nanoparticles", J. Phys. D J PHYS D APPL PHYS, 2013 , 46, 312001.

[27] R. Hergt, S. Dutz, M. Röder, "Effects of size distribution on hysteresis losses of magnetic nanoparticles for hyperthermia", J. Condens. Matter Phys., 2008, 20, 385214.

[28] M. Coïsson, G. Barrera, F. Celegato, L. Martino, S.N. Kane, S. Raghuvanshi, F. Vinai, P. Tiberto, "Hysteresis losses and specific absorption rate measurements in magnetic nanoparticles for hyperthermia applications", Biochim Biophys Acta Gen Subj BBA-GEN SUBJECTS, 2017, 1861, 1545-1558.

[29] M. Rezvani, P.R. Oskoui, A. Kianvash, "Preparation of Self-Catalyzing Sols in the $40SiO_2–30FeO–20FeO–20CaO–10Na_2O$ Glass System by Sol-Gel Method", ChemistrySelect, 2023, 8, 202204343.

[30] M. Rezvani, "The effect of complex nucleating agent on the physical and chemical properties of Li_2O-Al_2O_3-SiO_2 glass ceramic", Iran. J. Mater. Sci. Eng., 2010, 7, 300-312.

[31] M. Kiani Zitani, M. Rezvani, R. Asadi Tabrizi, "Crystallization, sinterability and microwave dielectric properties of CaO-SiO_2-Na_2O-MgO glass ceramics containing Fe_2O_3 and ZnO", Electron. Mater. Lett., 2014, 10, 131-137.

[32] R. Nariyal, P. Kothari, B. Bisht, "FTIR measurements of SiO_2 glass prepared by sol-gel technique", Chem. sci. trans., 2014, 3, 1064-1066.

[33] M. Stoia, R. Istratie, C. Păcurariu, Investigation of magnetite nanoparticles stability in air by thermal analysis and

[DOI: 10.22068/ijmse.3238]

FTIR spectroscopy, J. Therm. Anal. Calorim., 2016, 125, 1185-1198.
[34] P. Roonasi, A. Holmgren, "A Fourier transform infrared (FTIR) and thermogravimetric analysis (TGA) study of oleate adsorbed on magnetite nano-particle surface", Appl. Surf. Sci., 2009, 255, 5891-5895.
[35] Q.-Z. Chen, Y. Li, L.-Y. Jin, J.M. Quinn, P.A. Komesaroff, "A new sol–gel process for producing Na_2O-containing bioactive glass ceramics", Acta biomater, 2010, 10, 4143-4153.
[36] Z. Li, C. Chanéac, G. Berger, S. Delaunay, A. Graff, G. Lefèvre, "Mechanism and kinetics of magnetite oxidation under hydrothermal conditions", RSC Adv., 2019, 9, 33633-33642.
[37] S. Schwaminger, D. Bauer, P. Fraga-García, F. Wagner, S. Berensmeier, "Oxidation of magnetite nanoparticles: impact on surface and crystal properties", Cryst. Eng. Comm., 2017, 19, 246-255.
[38] R. Grau-Crespo, A.Y. Al-Baitai, I. Saadoune, N.H. De Leeuw, "Vacancy ordering and electronic structure of γ-Fe_2O_3 (maghemite): a theoretical investigation", J. Condens. Matter Phys., 2010, 22, 255401.
[39] E. Darezereshki, "Synthesis of maghemite (γ-Fe_2O_3) nanoparticles by wet chemical method at room temperature", Mater. Lett., 2010, 64, 1471-1472.
[40] X. Yang, P. Roonasi, R. Jolsterå, A. Holmgren, "Kinetics of silicate sorption on magnetite and maghemite: An in situ ATR-FTIR study", Colloids Surf., A Physicochem Eng. Asps., 2009, 343, 24-29.
[41] M. Gotić, G. Koščec, S. Musić, "Study of the reduction and reoxidation of substoichiometric magnetite", J. Mol. Struct., 2009, 924, 347-354.
[42] Z.K. Heiba, S.I. Ahmed, M.B. Mohamed, "Improved nonlinear optical and magnetic properties of Eu-doped nano-maghemite", J. Appl. Phys. A, 2022, 128, 415-423.
[43] A. El-Qanni, N.N. Nassar, G. Vitale, A. Hassan, "Maghemite nanosorbcats for methylene blue adsorption and subsequent catalytic thermo-oxidative decomposition: Computational modeling and thermodynamics studies", J. Colloid Interface Sci., 2016, 461, 396-408.
[44] Q. Gao, F. Chen, J. Zhang, G. Hong, J. Ni, X. Wei, D. Wang, The study of novel Fe_3O_4@ γ-Fe_2O_3 core/shell nanomaterials with improved properties, J. Colloid Interface Sci., 2009, 321, 1052-1057.
[45] A. Uheida, G. Salazar-Alvarez, E. Björkman, Z. Yu, M. Muhammed, "Fe_3O_4 and γ-Fe_2O_3 nanoparticles for the adsorption of Co^{2+} from aqueous solution", J. Colloid Interface Sci., 2006, 298, 501-507.
[46] C.-W. Chen, "Magnetism and metallurgy of soft magnetic materials", Courier Corporation, New York, USA, 2013, 240-263.
[47] A. Goldman, Handbook of modern ferromagnetic materials, Springer Science & Business Media, New York, USA, 2012, 851-867.
[48] Q. Chen, W. Chen, Y. Wang, B. Miao, "EPR NMR, and XPS study of $LaAlO_3$ phase transition with enhanced magnetic and Faraday rotation properties in glass-ceramics", J. Non Cryst. Solids, 2023, 43, 576-592.
[49] A. Fedotovs, A. Antuzevics, U. Rogulis, M. Kemere, R. Ignatans, "Electron paramagnetic resonance and magnetic circular dichroism of Gd^{3+} ions in oxyfluoride glass–ceramics containing CaF2 nanocrystals", J. Non Cryst. Solids, 2015, 429, 118-121.
[50] A. Yousefi, S. Seyyed Ebrahimi, A. Seyfoori, H. Mahmoodzadeh Hosseini, "Maghemite nanorods and nanospheres: synthesis and comparative physical and biological properties", j. Bionanosci., 2018, 30, 95-104.
[51] N. Chaudhari, S. Warule, S. Muduli, B. Kale, S. Jouen, B. Lefez, B. Hannoyer, S. Ogale, "Maghemite (hematite) core (shell) nanorods via thermolysis of a molecular solid of Fe-complex", Dalton Trans., 2011, 40, 8003-8011.
[52] T.-K. Van, H.G. Cha, C.K. Nguyen, S.-W. Kim, M.-H. Jung, Y.S. Kang, "Nanocrystals of hematite with unconventional shape-truncated hexagonal bipyramid and its optical and magnetic properties", Cryst. Growth Des., 2012, 12,

[DOI: 10.22068/ijmse.3238]

862-868.
[53] L. Wang, N.T. Nguyen, Z. Shen, P. Schmuki, Y. Bi, "Hematite dodecahedron crystals with high-index facets grown and grafted on one dimensional structures for efficient photoelectrochemical H2 generation", Nano Energy, 2018, 50, 331-338.

[DOI: 10.22068/ijmse.3238]